ELSEVIER

Tectonophysics 246 (1995) 225–243

TECTONOPHYSICS

The earthquake sequence of June 1992 near Saba, West Indies

William B. Ambeh, Lloyd L. Lynch

Seismic Research Unit, University of the West Indies, St. Augustine, Trinidad, Trinidad and Tobago

Received 18 January 1994; accepted 9 November 1994

Abstract

During June 1992, a minor earthquake swarm occurred close to the island of Saba, a small composite volcano which is the northernmost member of the inner volcanically active Lesser Antilles arc. The initial phase of the seismic activity was recorded at some permanent eastern Caribbean seismic stations, the nearest of which was located 55 km away. On 14 June 1992, a seismograph was installed on Saba to improve the detection and location capacities of the permanent network with regard to this swarm.

Sixty events were detected of which only fifteen could be located. The largest earthquake of the sequence occurred on 11 June 1992, had a duration magnitude of M_D 4.5 and was felt at Modified Mercalli intensities IV–V in Saba and III in St. Kitts. The epicentres exhibit a SW–NE trend and focal depths are mainly clustered in the range 10–16 km. A *b*-value of 0.73 was obtained for the sequence. Spectral analysis yielded various source parameters: moments in the range 0.38×10^{13}–23.66×10^{13} Nm, source radii from 87 to 126 m and stress drops from 1.3 to 79.9 bar. Moment increases with increasing magnitude while stress drop appears to decrease with decreasing seismic moment, similar to many other studies. Although the evidence as to the nature of the origin of this swarm is not conclusive, it seems to suggest a tectonic rather than volcanic origin.

1. Introduction

Saba is a small composite volcano whose summit, Mt. Scenery, rises to an altitude of 887 m, with a steep submarine slope indicating a possible height above the sea floor of about 1500 m. Surrounding Mt. Scenery are several isolated, steep-sloped peaks and domes. Saba is the northernmost island of the inner Lesser Antilles arc. The 700 km long Lesser Antilles island arc (Fig. 1) marks the eastern boundary of the Caribbean plate where the latter meets and is underthrust by Atlantic sea floor attached to the North American and/or the South American plate. While the inner Lesser Antilles arc is presently volcanically active, the outer arc represents an extinct limestone-capped pre-Miocene volcanic arc without any present-day volcanic hazard (Roobol et al., 1994).

At the beginning of June 1992, earthquakes were felt on a more or less regular basis in Saba. The largest earthquake of this sequence occurred on 11 June 1992, had a duration magnitude of 4.5 and was felt at Modified Mercalli (MM) intensities of IV–V and III in Saba and St. Kitts, respectively. A few of the earthquakes were large enough to be detected by instruments of the Eastern Caribbean Seismic Network operated by the Seismic Research Unit of the University of the West Indies, Trinidad, the "Observatoires Géophy-

SSDI 0040-1951(94)00254-1

siques" in Martinique and Guadeloupe, and the Department of Geology of the University of Puerto Rico, Mayaguez. However, there was no seismic station on Saba at this time and the nearest seismograph was about 55 km away.

Although the occurrence of swarms of felt

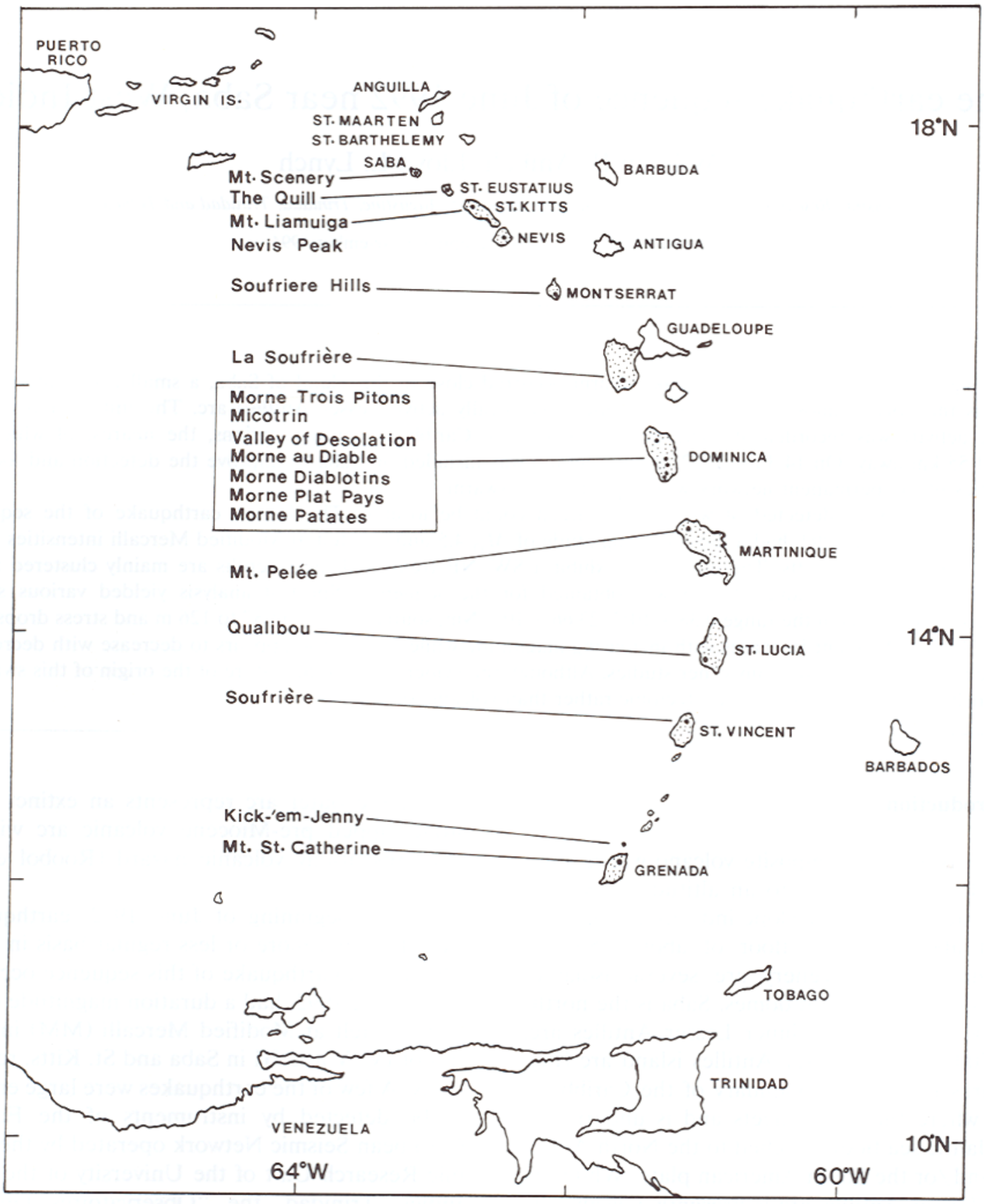

Fig. 1. Some active and potentially active volcanoes in the Lesser Antilles.

earthquakes beneath or close to volcanic centres in the Lesser Antilles is a fairly common phenomenon (e.g., Nevis Peak, Nevis, 1831–1835, 1926, 1947–1948, 1950–1951, 1961–1962; Soufrière Hills, Montserrat, 1879–1900, 1933–1938, 1966–1967, 1989, 1992; La Soufrière, Guadeloupe, 1797, 1809–1912, 1836–1937, 1956, 1976–1977; etc.), we are not aware of any series of felt earthquakes that have occurred close to Saba for a very long time. The occurrence of a series of earthquakes close to a volcano does not necessarily mean that the volcano is going to erupt since volcanoes are located in such geologically unstable areas that certain signals may reveal a significant change in comparison with the background activity level without necessarily relating to the rise of molten material at depth. However, since changes in the pattern of earthquake occurrence, mainly involving an increase, have also been noted to occur prior to eruptions at several volcanoes (e.g., Sawada et al., 1989; Mori et al., 1989; Barquero et al., 1992), the government of the Netherlands Antilles, of which Saba is part, asked the Seismic Research Unit to provide technical assistance in monitoring the earthquake sequence. In order to improve the detection and location capabilities of the permanent eastern Caribbean network for earthquakes occurring in the vicinity of Saba, a three-component seismograph was installed at the Govern-

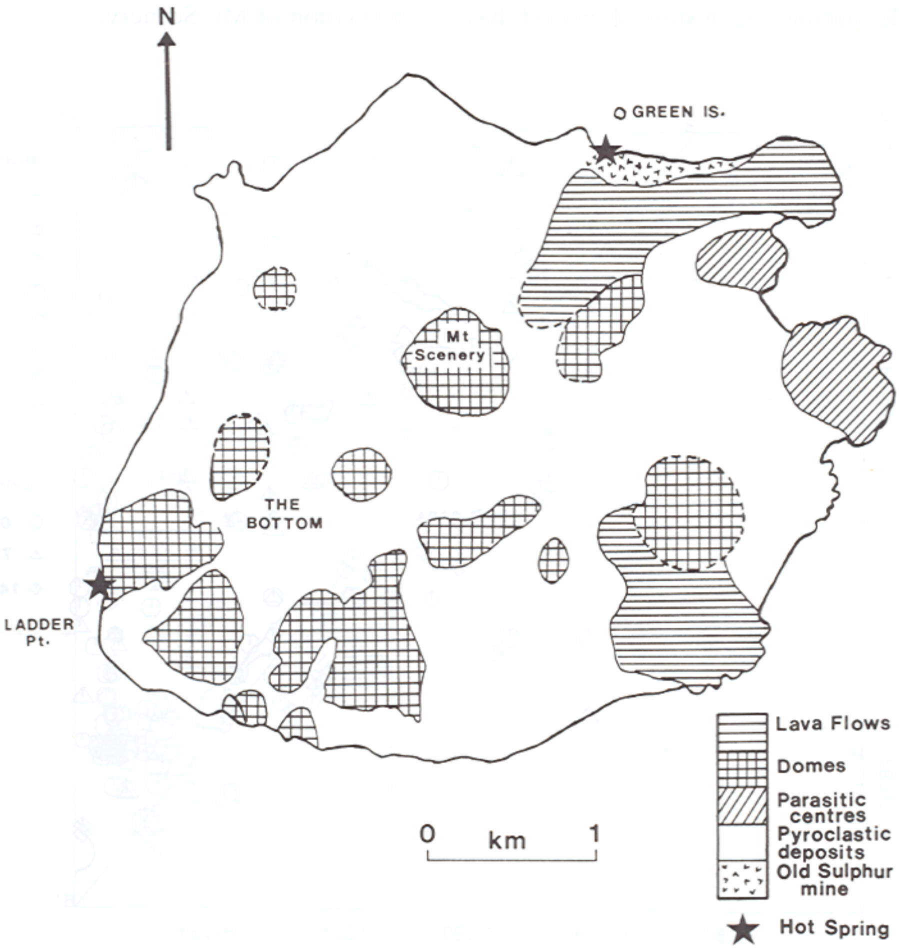

Fig. 2. Geological sketch map of Saba (based on Westermann and Kiel, 1961; Roobol et al., 1994).

ment Administration Building, The Bottom, Saba, on 14 June 1992. Two weeks later, the seismometer was moved to the summit of Mt. Scenery and the signal telemetered to Trinidad by VHF radio and microwave links. Additional telemetered stations were also set up in Statia, St. Maarten and St. Barthelemy.

This paper describes the earthquake sequence in detail.

2. Volcanological setting

Although some Lesser Antillean volcanoes have been the sites of very large and destructive eruptions (e.g., Mt. Pelée, Martinique, 1902; Soufrière, St. Vincent, 1902), the most common eruption style during the historical period has been one involving phreatic/phreatomagmatic activity (Smith and Roobol, 1994).

The geology of Saba was first described in detail by Westermann and Kiel (1961). Roobol et al. (1994) delineated the volcanic hazards from geological mapping and studies of stratigraphic sections. A simplified geological map of Saba is shown in Fig. 2.

Before about 70,000 yr ago, Saba consisted of a complex of many old Pelean domes surrounded by lithified andesitic lava flows, agglomerates and tuffs. During the past 70,000 yr, Mt. Scenery has been built on top of an earlier Pelean dome complex by many different eruptive styles which have produced a wide variety of rock types and deposits. Flank eruptions, which led to the creation of the Saba domes, also accompanied the formation of Mt. Scenery.

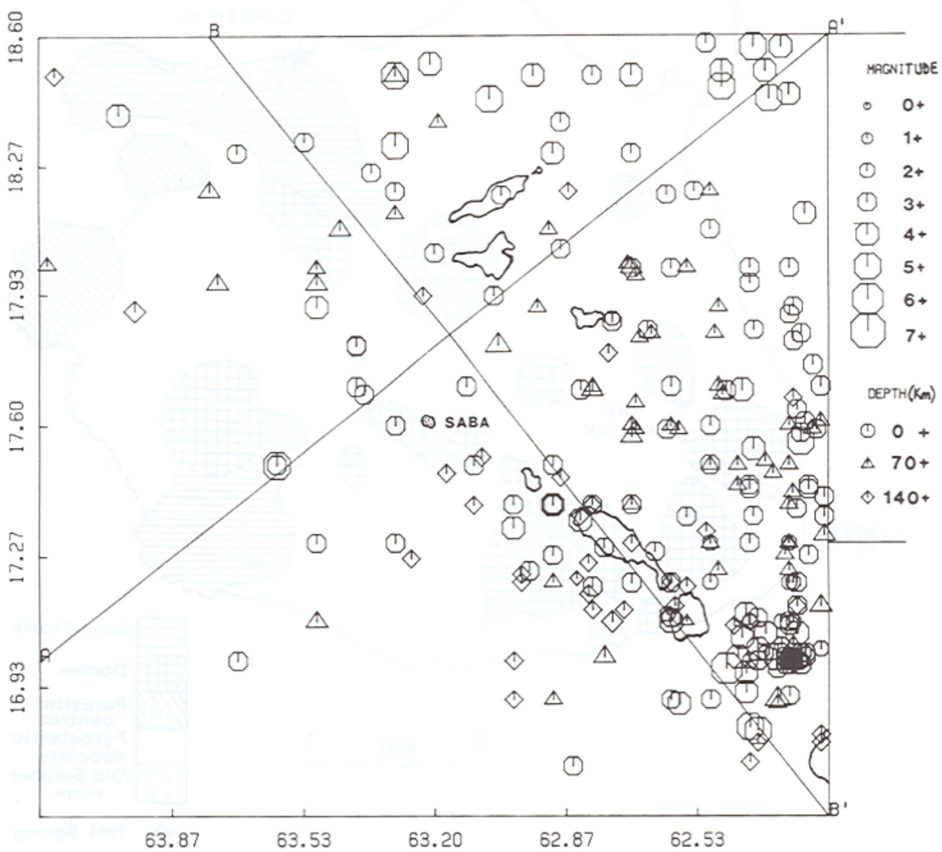

Fig. 3. Seismicity of the Saba area: 01/01/1964–31/05/1992.

The first eruptions of Saba's volcano may date as far back as the middle or Late Pleistocene while the last volcanic processes may have continued until the middle Holocene (Westermann and Kiel, 1961). The dominant eruption pattern was that of Pelean type which resulted in the production of nuées ardentes of block and ash and dense andesite deposits. Radiocarbon dating of andesite surge deposits containing accretionary lapilli found beneath The Bottom suggest that a Pelean eruption may have occurred on Saba about 300 yr ago, just shortly before European settlement (Roobol and Smith, 1989). The only current manifestations of volcanic activity are two minor hot springs at sea level near Ladder Point and opposite Green Island.

3. Seismicity of the Saba area before the June 1992 sequence

In Fig. 3 a plot is shown of earthquake epicentres within a 1° radius centred on Saba for the period January 1964 to May 1992. The event parameters were extracted from the bulletins of the Seismic Research Unit, the International Seismological Centre (UK) and the National Earthquake Information Centre (USA). The location accuracies and detection thresholds during this period have changed with time as a result of changes in seismic station geometries and densities.

Earthquakes are scattered throughout the area, with a higher density beneath and to the east of the arc platform. The cluster of seismicity centred around 62.4° W, 17.0° N is due mainly to the aftershocks of the 16 March 1985 m_b 6.1 earthquake. Few earthquakes are located close to Saba and towards the western parts. This spatial variation in seismicity may be partially attributable to the fact that some of the islands in the area such as Saba, St. Maarten, Anguilla, Statia and St. Barthelemy have not been permanently instrumented throughout this period. Temporary seismic stations were operated on most of these islands from 1975 to 1982 by the Lamont–Doherty Observatory of Columbia University, New York (Murphy and McCann, 1979).

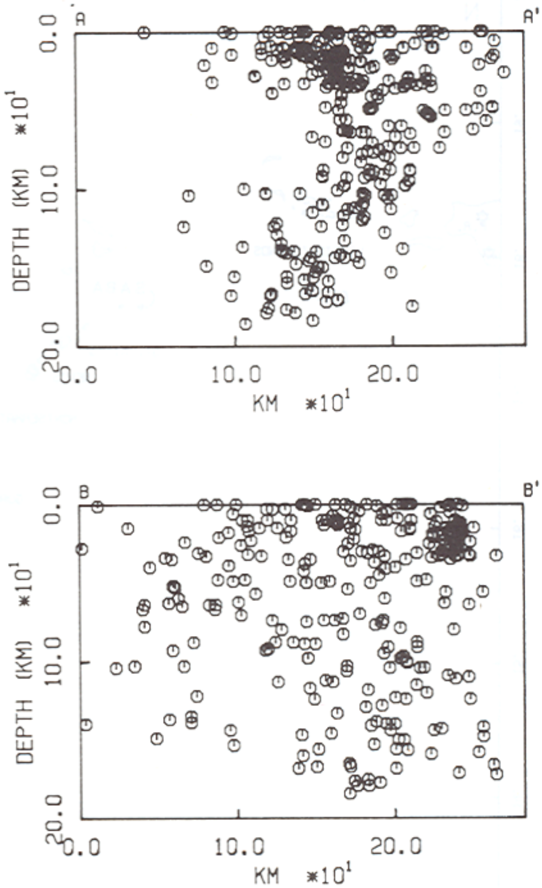

Fig. 4. Hypocentres of earthquakes projected onto vertical planes AA' and BB' (see Fig. 3).

In Fig. 4 earthquake hypocentres are shown, projected onto planes AA′ and BB′, approximately perpendicular to and parallel to the arc, respectively. Earthquake focal depths range from near-surface to about 190 km and clearly define a down-going seismic zone that dips about 50° to the southwest and has a thickness of about 65 km (Fig. 4a). The earthquakes of this down-going zone are presumably produced along a subducted portion of the North American plate.

4. Seismicity close to Saba from June 1992

4.1. Instrumentation

During the first two weeks of occurrence of the sequence of earthquakes near Saba, the clos-

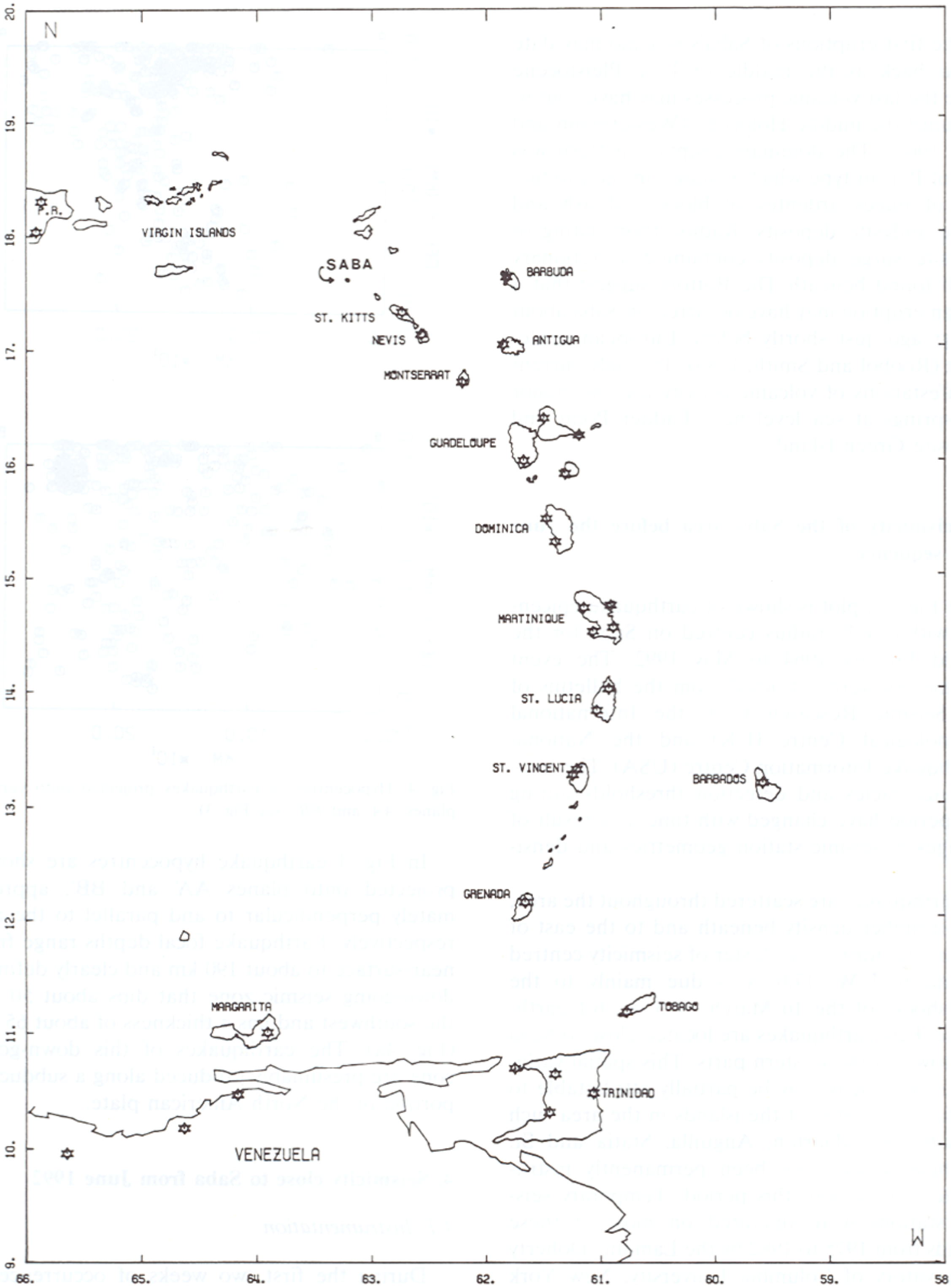

Fig. 5. Some permanent stations (stars) of the eastern Caribbean Seismic Network.

est seismic station of the permanent telemetered short-period eastern Caribbean Seismic network was located about 55 km to the southeast, in St. Kitts (Fig. 5). On 14 June 1992, a Sprengnether S-6000 three-component 2 Hz seismometer was installed in the Government Administration Building in The Bottom, Saba, in order to improve our detection and location capacities with regard to the sequence. The signals from the three components (oriented up, north and east) were amplified at two different gains in order to avoid saturation problems for the slightly larger events while also recording the smaller ones. The low-gain signals were also passed through low-pass filters with 3 dB points at 12.5 Hz. The amplified/filtered signals were then fed into an analogue-to-digital board mounted in a Laptop computer and digitized at a rate of 100 samples/s and 12-bit resolution. Earthquake recording on the computer is based on an event-triggering software. The seismograph station was given the code SAB.

Concurrently with the operation of the three-component event-triggered recorder, a vertical component Marks Product L4C seismometer connected to a Sprengnether MK 400 drum recorder was also used to provide direct visual display.

On 30 June 1992, the seismometer was moved from The Bottom to the summit of Mt. Scenery and the signal telemetered to Trinidad via VHF radio and microwave links. Additional telemetered stations were also set up on St. Maarten and Statia by the SRU and on St. Bathelemy by the "Observatoire Géophysique" of Guadeloupe.

4.2. Space and time distribution of events

Temporal variation of the Saba sequence

Since the commencement of the sequence of earthquakes near Saba, a total of 60 events was detected. In Fig. 6 a histogram of the variation of the daily count of earthquakes is shown. This was constructed using counts at the St. Kitts stations before 14 June and at the Saba station after 14 June, and is, consequently, not a reflection of the "true" temporal variation because of the different detection thresholds. The detection threshold was lowered considerably after the installation of the Saba seismic station on 14 June, 1992. Twelve earthquakes were detected before 14 June (all of which were large enough to be located) and 48 were detected after 14 June. Although the highest number of earthquakes per day was observed on 15 and 16 June, the sequence was definitely most intense on 11 June, before the installation of the Saba seismograph. No earthquakes were detected after the Saba station was moved from The Bottom to the summit of Mt. Scenery and this was most probably due to the fact that this new station was operated at a lower gain because of the high background noise level.

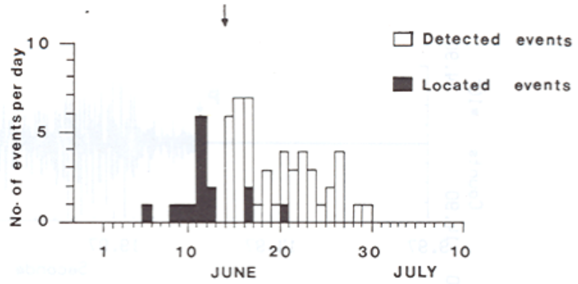

Fig. 6. Temporal variation of the daily number of events of the Saba earthquake swarm (arrow shows day of installation of Saba seismograph).

Swarms, mainshock–aftershock sequences and classification of near-volcano earthquakes

Earthquakes that are concentrated in both space and time can be classified either as swarms or mainshock–aftershock sequences. An earthquake swarm is a series of shocks none of which appreciably exceeds the rest in magnitude (Evison, 1977). Swarms are common in volcanic regions (volcanic swarms) (e.g., Eiby, 1966) but also occur in many non-volcanic regions (tectonic swarms) (e.g., Frankel et al., 1980). A mainshock–aftershock sequence involves the occurrence of a moderate or large earthquake followed by a series of smaller events close to the original source region. Smaller earthquakes called foreshocks may sometimes precede the main event.

Various classification schemes for earthquakes occurring close to volcanoes have been proposed and most of these are based on the nature of seismic waveforms recorded at the surface (e.g.,

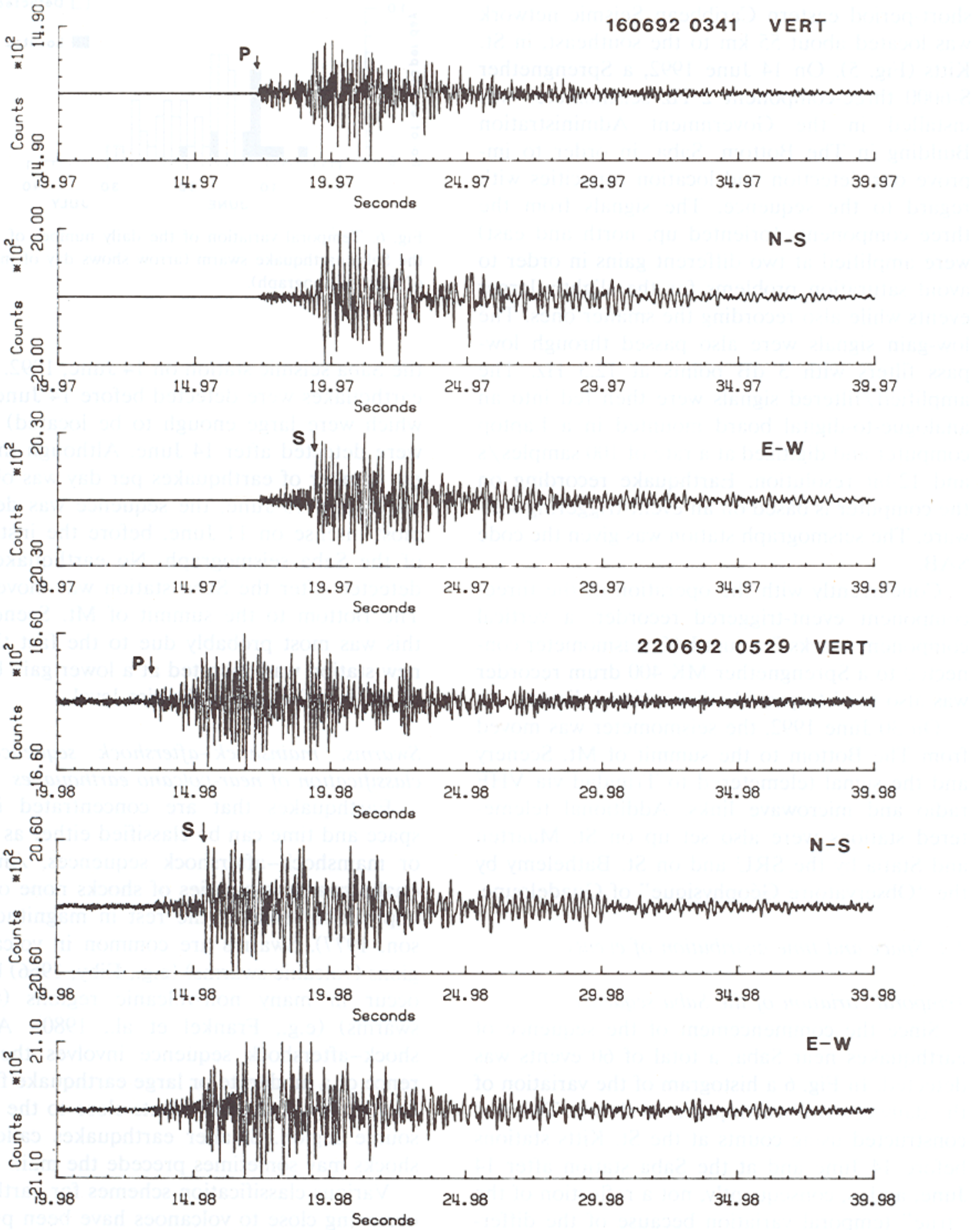

Fig. 7. Examples of waveforms for two Saba sequence events recorded at station SAB (top: 160692 0341 UTC, bottom: 220692 0529 UTC).

Minakami, 1974; Latter, 1979). Waveform properties considered include the nature of the P and/or S phase onset, the frequency content and the signal duration. Most of these classification schemes essentially distinguish between three broad categories of near-volcano earthquakes: tectonic, volcano-tectonic and volcanic. However, it is often difficult to differentiate between events of volcano-tectonic origin and those of tectonic origin. A "volcanic" earthquake is considered as one which occurs in the vicinity of an "active" volcano and whose origin is directly related to processes such as magma injection or gas expansion. This relationship is, however, usually hard to demonstrate.

Examples of waveforms for events of this sequence recorded at the Saba station are shown in Fig. 7. In general, the P and S phase onsets are clear although the P onsets are often emergent. No significant variation in the nature of the waveforms was observed during the recording period.

Spatial distribution of hypocentres

Locations were calculated for all earthquakes recorded by four (4) or more seismic stations with a minimum of six (6) P and/or S phases using the computer program WURSTMACHINE (Beckles et al., 1977), together with the LADLE velocity model (LADLE Study Group, 1983). This resulted in a total of fifteen (15) earthquakes being located of which only three (3) occurred after the installation of the seismic station on Saba. The hypocentral parameters for these events are probably associated with relatively large errors which vary depending on whether the locations were calculated with arrival times at stations in one, two, three or four quadrants, and the distance of the nearest station. Location accuracies for pre-14 June epicentres may be of the order of ± 15 km while for post-14 June events, whose locations were determined with arrival times at the permanent seismic network stations supplemented with arrival time data at SAB, are probably slightly better. Also, the larger events, which were recorded by both the Seismic Research Unit and the University of Puerto Rico stations, obviously have better location errors because of a better azimuthal coverage. Depth accuracies for both periods are also different, with those for the post-14 June period being better.

Analysis of the effects of inadequate spatial distribution of seismic stations on hypocentral locations using "synthetic" events seems to suggest that these errors may be much larger. However, given the fact that the average $S-P$ time for these events recorded at SAB was 1.94 ± 0.17 s (if we assume a surface focus, a $V_p/V_s \approx 1.75$, a $V_p = 6$ km/s, a rough estimate of the distance between the station and the earthquakes is $8 \times 1.94 \approx 15$ km), we feel that actual errors in the hypocentral parameters are substantially less, probably of the order of ± 10 km or better, especially for the events recorded by both the SRU and the University of Puerto Rico stations and those that occurred after the installation of SAB.

Magnitudes were estimated from signal duration using the formula developed for the eastern Caribbean by Shepherd and Aspinall (1983):

$$M_D = -0.705 + 2.073 \log_{10} \tau + 0.0018\, R$$

where τ is signal duration in seconds and R is hypocentral distance in kilometers. Signal duration magnitudes were calculated for all the detected earthquakes and their variation is shown in Fig. 8. Magnitudes range from 1.4 to 4.5, with the differential between the largest and the second largest shock being 0.7 magnitude units. The two largest events occurred on 11 June, the second largest event preceding the largest one by 2.5 hours. The great majority of earthquakes, however, had magnitudes in the range M_D 2.0–2.5. The largest shock [M_D 4.5, m_b 4.4, M_{SZ} 3.8 (NEIC)] was felt at Modified Mercalli intensities IV–V in Saba and III in St. Kitts. The temporal variation of magnitudes during the sequence (Fig. 8B) again reflects the lowering of the detection threshold as a result of the installation of the Saba seismograph on 14 June.

In Fig. 9a and b plots are shown of the epicentres of the Saba sequence earthquakes obtained by single event location and joint hypocentre determination, respectively. Most of the epicentres are located within 15 km of Saba and a poor SW–NE trend in epicentres seems to be apparent (Fig. 9a). This pattern of locations may be an artifact of the geometry of the seismograph array since all the seismic stations used in the location process (except for some of the largest events) are situated to the east and southeast of Saba. The depths of the earthquakes projected onto two planes parallel to and perpendicular to the general trend of the epicentres are shown in Fig. 9c and e. The earthquakes occur at depths from 1 to 23 km, with most of them clustering around 7 to 12 km. It must again be emphasized that the focal depths, especially those for events which occurred before the installation of SAB, are relatively poor given the absence of a station within one focal depth of the earthquakes.

In an attempt to better define the spatial pattern of the sequence, hypocentres were also computed using a variant of the Joint Hypocentre Determination (JHD) method (Beckles and Shepherd, 1988). The JHD locations and depth cross sections are shown in Fig. 9b, d and f. The poor SW–NE trend in epicentres observed with the standard locations is better defined with the JHD locations but most of the focal depths are now larger, in the range 10–16 km. The observed SW–NE-trending seismicity feature may thus be real but we cannot over conclude from this at the moment.

The hypocentral parameters calculated using the single event location (SEL) and the JHD methods are listed in Table 1.

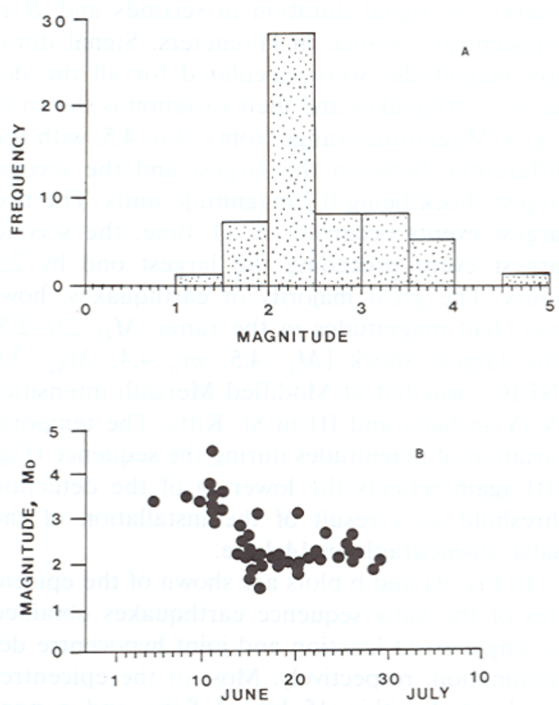

Fig. 8. Temporal and frequency variation of magnitude for Saba swarm. (a) Histogram of magnitude variation. (b) Temporal variation of event magnitudes.

4.3. Focal mechanism

Tectonic earthquakes generate first motions which exhibit a particular quadrantal distribution of compressions and dilatations on the focal sphere. Unfortunately, most of the events were so small that the number of stations able to record them does not result in a sufficient number of first motions to allow the determination of well-constrained focal mechanisms.

A plot of first motions for the largest event of the sequence on an equal area projection of the lower focal hemisphere yields a poorly constrained focal mechanism which seems to be consistent with reverse faulting (Fig. 10). However, none of the nodal planes has a strike with the same trend as the epicentres. For four events with very clear P-wave onsets on the Saba station, two compressions and two dilatations were documented, possibly indicating that the mechanism was not constant for all the earthquakes but may have changed with time and/or space. This may also indicate that the Saba sequence events are not directly attributable to magma movement since seismic signals originating from the propagation of fluid-driven tensile cracks generate compressive first motions everywhere (Aki, 1984).

4.4. b-value

The frequency of occurrence of earthquakes as a function of magnitude is commonly expressed as:

$$\log N_c = a - bM$$

which is a slightly modified form of the Gutenberg–Richter relation (Gutenberg and Richter, 1954), where N_c is the cumulative number of earthquakes of magnitude greater than or equal to M and a and b are constants. The constant a depends on the sample size while b, commonly called the b-value, is a measure of the relative numbers of large and small events in the sample. In Fig. 11 a plot is shown of log N_c versus M for a magnitude interval of 0.5 and utilizing all the earthquakes detected during the sequence. A b-

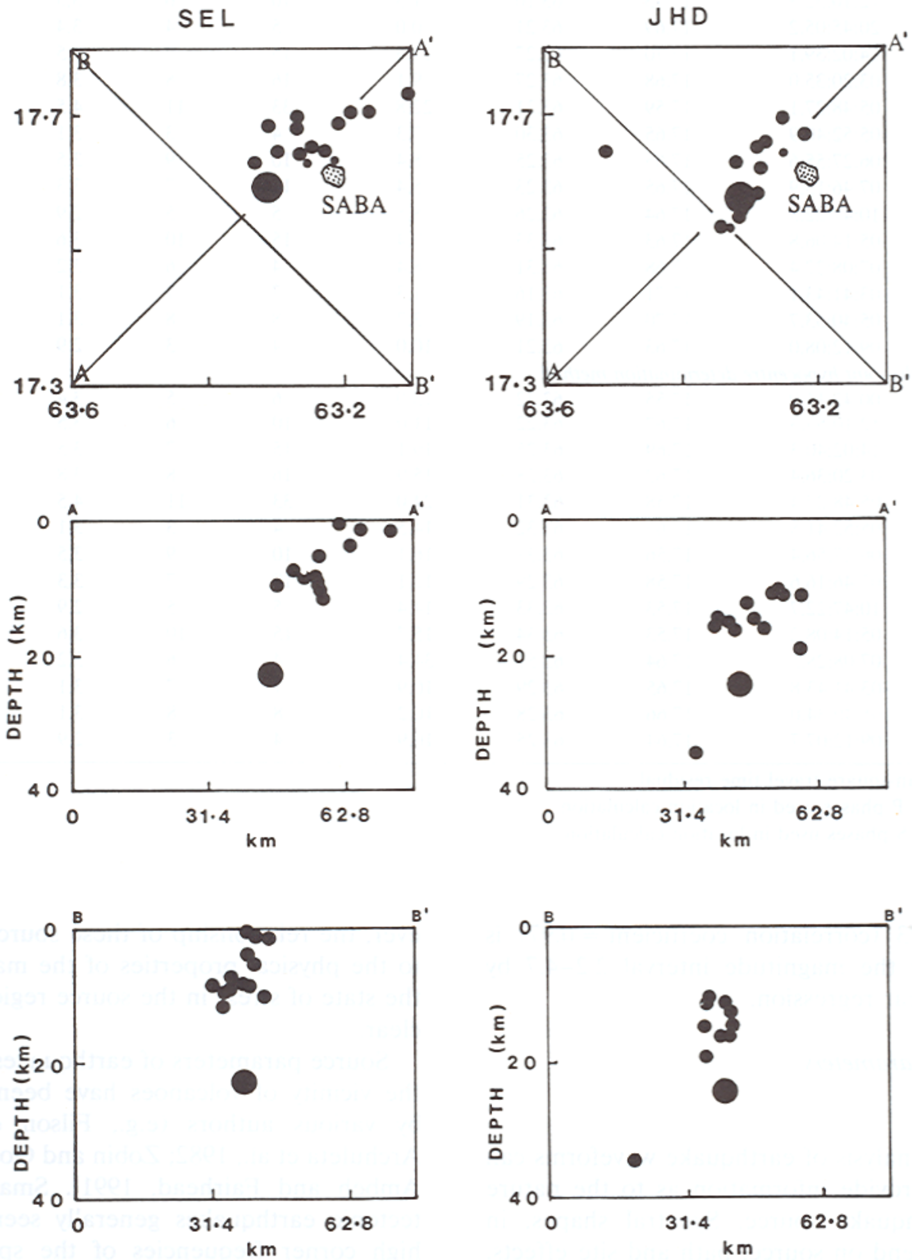

Fig. 9. Epicentre and depth cross section plots for hypocentres obtained by the single event location (*SEL*) and the joint hypocentre determination (*JHD*) techniques.

Table 1
Hypocentral parameters of Saba events

Date (d.mon.yr)	Origin time (h:min:s)	Lat (° N)	Long (° W)	Depth (km)	N_p	N_s	M_D	Rms (s)
A. Obtained by the single event location method								
05.06.92	00:42:11.0	17.64	63.26	8.2	6	5	3.4	0.45
08.06.92	12:10:52.3	17.73	63.10	1.5	10	6	3.5	0.83
09.06.92	20:45:05.2	17.69	63.21	0.0	5	4	3.4	0.36
10.06.92	14:02:39.1	17.70	63.27	11.5	15	7	3.5	0.50
11.06.92	03:20:35.0	17.68	63.27	9.1	16	8	3.8	0.62
11.06.92	05:48:27.1	17.59	63.31	22.8	33	11	4.5	0.65
11.06.92	05:52:40.9	17.65	63.30	7.3	4	3	3.1	0.29
11.06.92	06:27:55.6	17.65	63.25	8.4	10	9	3.5	0.68
11.06.92	07:46:15.9	17.65	63.23	5.4	10	7	3.3	0.39
11.06.92	10:47:22.5	17.64	63.26	8.5	5	5	2.9	0.28
12.06.92	05:14:06.8	17.63	63.33	9.4	15	10	3.6	0.48
12.06.92	07:08:27.4	17.68	63.31	8.4	4	6	3.2	0.67
16.06.92	03:41:43.1	17.71	63.16	1.3	7	7	3.1	0.29
16.06.92	05:40:33.7	17.70	63.19	3.7	8	8	3.1	0.39
20.06.92	09:12:08.0	17.63	63.21	10.0	4	3	2.9	0.24
B. Obtained by the joint hypocentre determination method								
05.06.92	00:42:11.9	17.55	63.32	15.0	6	5	3.4	0.11
08.06.92	12:10:53.3	17.67	63.22	11.0	10	6	3.5	0.78
10.06.92	14:02:40.3	17.69	63.25	19.1	15	7	3.5	0.23
11.06.92	03:20:36.4	17.62	63.28	15.9	16	8	3.8	0.40
11.06.92	05:48:27.4	17.58	63.31	24.0	33	11	4.5	0.51
11.06.92	05:52:41.8	17.63	63.32	14.5	4	3	3.1	0.39
11.06.92	06:27:56.4	17.56	63.31	16.1	10	9	3.5	0.41
11.06.92	07:46:16.6	17.58	63.29	12.1	10	7	3.3	0.22
11.06.92	10:47:22.7	17.53	63.33	14.4	5	5	2.9	0.42
12.06.92	05:14:08.2	17.53	63.34	15.7	15	10	3.6	0.34
12.06.92	07:08:28.5	17.64	63.51	34.4	4	6	3.2	0.47
16.06.92	03:41:43.8	17.65	63.29	10.9	7	7	3.1	0.26
16.06.92	05:40:34.0	17.66	63.28	10.2	8	8	3.1	0.35
20.06.92	09:12:07.7	17.64	63.25	10.9	4	3	2.9	0.32

Rms = root-mean-square travel time residual.
N_p = number of P phases used in location calculation.
N_s = number of S phases used in location calculation.

value of 0.73 (correlation coefficient = 0.97) is obtained for the magnitude interval 2.2–4.7 by standard linear regression.

4.5. Source parameters

Introduction

Spectral analysis of earthquake waveforms can sometimes provide information as to the nature of the earthquake source. Spectral shapes, in general, depend on source, path and site effects. In particular, parameters such as moment, source length and stress drop can be determined. However, the relationship of these source parameters to the physical properties of the material and to the state of stress in the source region is not very clear.

Source parameters of earthquakes occurring in the vicinity of volcanoes have been investigated by various authors (e.g., Filson et al., 1973; Archuleta et al., 1982; Zobin and Gorelchik, 1982; Ambeh and Fairhead, 1991). Small magnitude tectonic earthquakes generally seem to possess high corner frequencies of the spectrum (e.g., Madariaga, 1976; Boatwright, 1980; Frankel, 1982). On the other hand, small-magnitude vol-

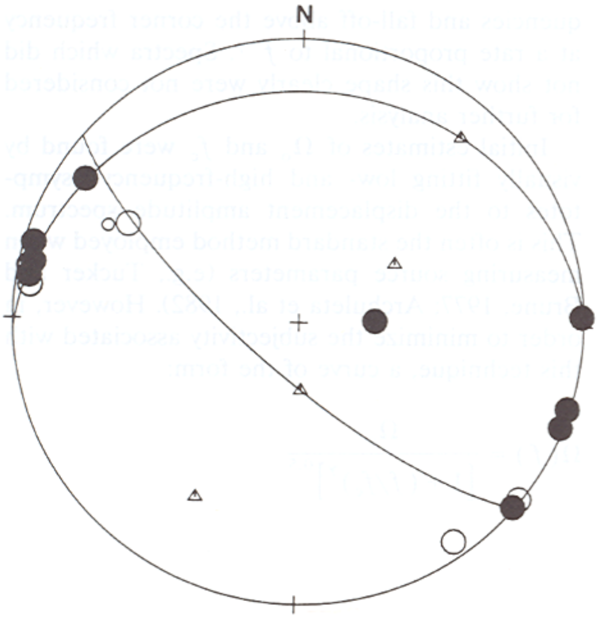

Fig. 10. Focal mechanism for event of 11/06/92 0548 UTC (• represent compressional first motions and ○ dilatations; lower hemisphere projection).

canic earthquakes often exhibit narrow spectral peaks and low corner frequencies. Zobin (1979) and Zobin and Gorelchik (1982) in an investigation of earthquakes occurring at Tolbachik volcano, found a systematic change in the spectral content of waveforms prior to eruptions.

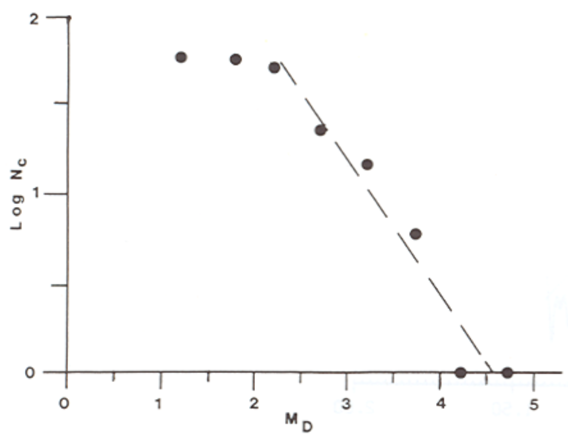

Fig. 11. Frequency–magnitude variation for Saba swarm events.

Most theoretical models of the seismic source predict a far-field displacement amplitude spectrum for body waves characterized by a constant level, Ω_o, at low frequencies up to a corner frequency, f_c, and then a decay proportional to $f^{-\gamma}$ $(\gamma > 1.5)$ for frequencies higher than f_c. Far-field spectral parameters (Ω_c, f_c) can be related to source parameters seismic moment (M_o), source radius (r) and stress drop $(\Delta\sigma)$ by the following formulae:

$$M_o = \frac{4\pi\rho\beta^3 R\Omega_o}{2\phi} \tag{1}$$

$$r = \frac{0.21\beta}{f_c} \tag{2}$$

$$\Delta\sigma = \frac{7}{16}\frac{M_o}{r^3} \tag{3}$$

where ρ is the density of the medium, R is hypocentral distance, β is S-wave velocity and ϕ accounts for the S-wave radiation pattern. The factor of 2 in the denominator of Eq. (1) corrects to a full-space by accounting for the free surface amplification due to reflection (normally taken as 2 for pure SH-waves). Eq. 1 is from Thatcher and Hanks (1973) (the S-wave velocity should be replaced by the P-wave velocity for P-wave spectra) while (2) and (3) are taken from Madariaga (1976).

Method

Spectra were only calculated for unclipped S-waves recorded on both horizontal components of SAB. To calculate spectra, a least squares baseline trend was first removed from the seismogram time series, then a portion of the S-wave signal of sufficient length to encompass the maximum without, if possible, including significant scattered energy or any other distinct phases, was chosen. Sample lengths varied from 3 to 6 seconds, with the main factor determining the choice of window lengths being the duration of signal with amplitude comparable to the maximum amplitudes.

A cosine taper was applied to ten samples at the front and end of the signal window. The tapered time series was then padded with zeroes to the nearest integer power of 2 and then Fourier transformed using the Fast Fourier Transform (FFT) algorithm. The Fourier transform of the sample was corrected for instrument response to give the displacement amplitude spectrum, corrected for noise, smoothed three times using a weighted five-point running mean, and displayed on log–log plots. No correction for attenuation was made but the possible effects of this on the results obtained will be discussed.

Spectra are generally not considered reliable outside the frequency bands 1.0–12.5 and 1.0–25.0 Hz for the low- and high-gain signals, respectively.

Almost all the observed spectra are characterized by a constant low-frequency level that extends from the corner frequency to lower frequencies and fall-off above the corner frequency at a rate proportional to $f^{-\gamma}$. Spectra which did not show this shape clearly were not considered for further analysis.

Initial estimates of Ω_o and f_c were found by visually fitting low- and high-frequency asymptotes to the displacement amplitude spectrum. This is often the standard method employed when measuring source parameters (e.g., Tucker and Brune, 1977; Archuleta et al., 1982). However, in order to minimize the subjectivity associated with this technique, a curve of the form:

$$\Omega(f) = \frac{\Omega_o}{\left[1 + (f/f_c)^{\gamma}\right]^{0.5}}$$

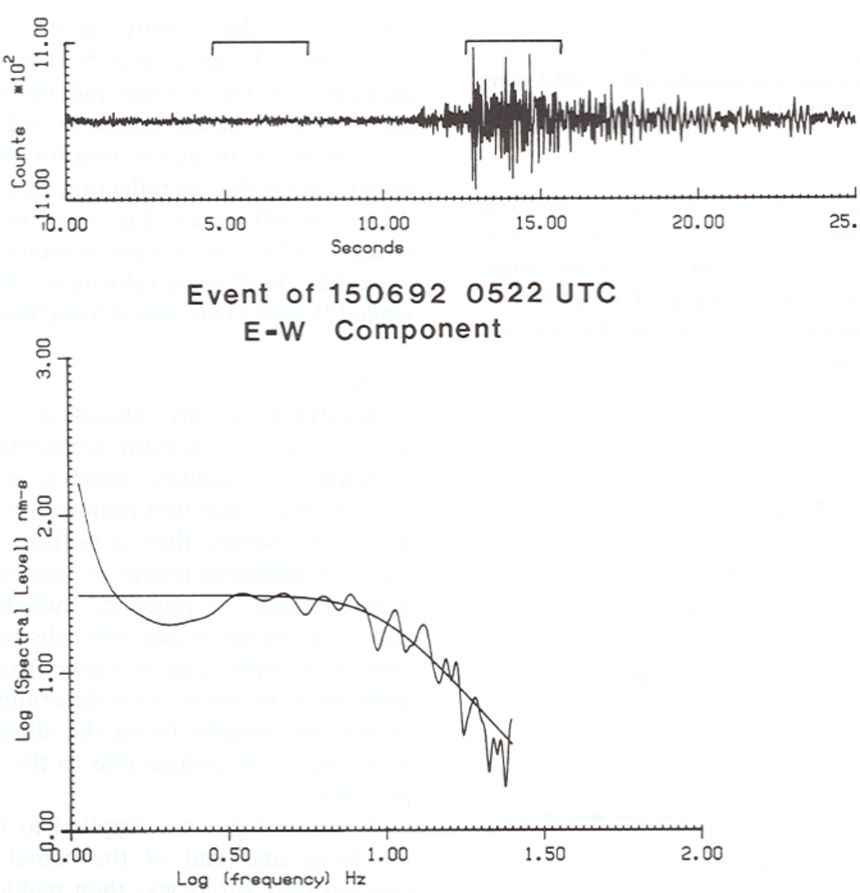

Fig. 12. An example of a seismogram, corresponding displacement amplitude spectrum and theoretical fit.

was then fitted to the spectrum by iterative non-linear least squares using the visual estimates as starting values. An example of a spectrum with superimposed theoretical fit is shown in Fig. 12. In general, the theoretical fits to the observed spectra were quite good. Source parameters moment, radius and stress drop were then obtained using Eqs. (1)–(3), assuming an average crustal density of 2750 kg/m^3 and S-wave velocity of 3.5 km/s. Since focal mechanisms were not available for each individual event, a root-mean-square (rms) average S-wave radiation pattern correction of 0.62 (Aki and Richards, 1980, p. 120) was used.

Results

Calculated spectral and source parameters are listed in Table 2. Corner frequencies are found in the range 5.7–12.0 Hz. All the spectra were found to roll off faster than $\gamma = 5$ and this is consistent with other observations of high frequency fall-off rates for microearthquakes (e.g., Iio, 1992). Seismic moments lie between 0.38×10^{13} and 23.66×10^{13} Nm. The calculated source radii are in the range 87–126 m while stress drops vary from 1.3 to 79.9 bar.

In Fig. 13 a plot of log moment versus magnitude (Fig. 13a), log source radius (Fig. 13b) and log stress drop (Fig. 13c) is shown. Moment increases with increase in magnitude as expected

Table 2
Average spectral and source parameters for Saba earthquakes

Date (d:mon:yr)	Time (h:min)	M_D	M_o ($\times 10^{13}$ Nm)	f_c (Hz)	r (m)	$\Delta\sigma$ (bar)
15.06.92	01:25	2.6	1.27	7.7	95.1	6.6
15.06.92	04:25	2.2	0.46	8.2	89.4	2.8
15.06.92	05:22	2.3	0.48	8.8	87.7	3.7
15.06.92	08:59	1.8	1.12	7.6	96.4	5.9
16.06.92	03:41	3.1	23.66	6.6	109.8	79.9
16.06.92	06:27	2.2	0.57	7.5	97.6	2.7
16.06.92	08:32	2.2	0.42	12.0	63.1	8.7
18.06.92	07:15	2.2	0.72	7.5	97.3	3.5
19.06.92	06:06	2.0	0.42	6.4	113.2	1.3
20.06.92	06:54	1.7	0.38	7.1	102.0	1.6
20.06.92	07:11	1.9	0.41	7.9	93.1	2.3
20.06.92	09:11	3.1	18.47	5.7	125.8	39.9
21.06.92	09:50	2.1	1.03	6.8	106.4	3.7
22.06.92	05:29	2.2	2.32	8.1	90.5	13.9
26.06.92	08:23	2.0	0.80	7.9	92.3	4.7

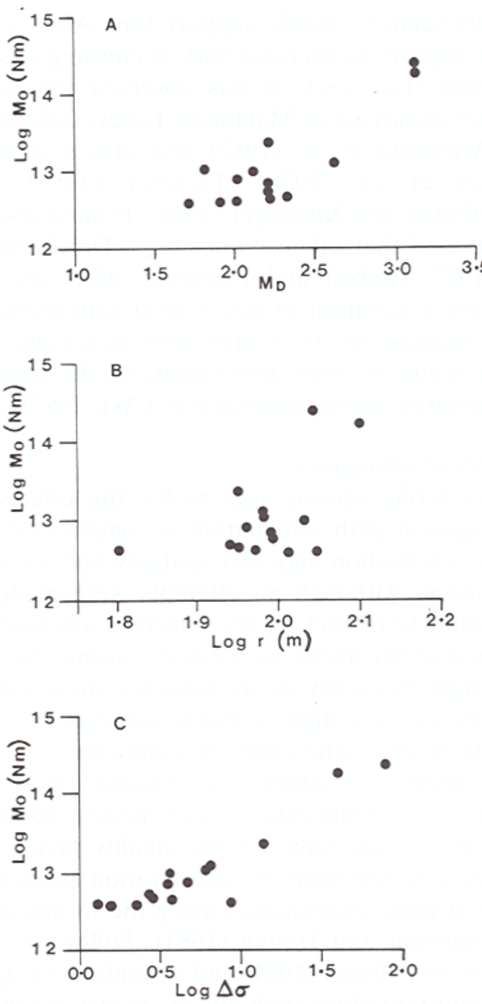

Fig. 13. Moment as a function of magnitude (M_D), source radius (r) and stress drop ($\Delta\sigma$).

and the equation of the least squares best fitting straight line (correlation coefficient = 0.84) is given by:

$$\log M_o = 1.17 M_D + 10.40$$

Source radius appears to change with changing seismic moment although the trend is not a glaring one (Fig. 13b). Pearson (1982), from a study of earthquakes accompanying hydraulic fracturing in a Hot Dry Rock geothermal reservoir, concluded that log seismic moment and log source radius are linearly related for earthquakes with moments ranging from 10^5 to 10^{20} Nm. Our results seem to mildly support this. Also, stress drop appears to decrease with decreasing seismic moment (Fig. 13c), as was observed for earthquakes occurring at Mammoth Lakes, California, by Archuleta et al. (1982) and others such as Bakun et al. (1976), Fletcher (1980) and Scherbaum and Kisslinger (1984). It must also be mentioned that other studies (e.g., Del Pezzo et al., 1987; Ambeh and Fairhead, 1991) did not observe a variation of stress drop with moment. This increase of stress drop with increasing moment seems to imply non-validity of the concept of similarity among earthquakes (Aki, 1967).

Effects of attenuation

Correcting seismic spectra for the effects of propagation path attenuation is complicated because attenuation may vary spatially and/or with frequency. Although no attempts were made in this study to correct for the effects of attenuation because of the above-mentioned reasons, the fact that high-frequency decay rates for these earthquakes are very high probably suggests that the effects of attenuation may be significant.

In order to examine the possible effects of attenuation on the estimates of spectral parameters, an average value of the quality factor, Q, was determined from the acceleration spectra of some of these earthquakes using the formulation of Anderson and Hough (1984). Following Anderson and Hough (1984) and assuming that Q is both constant along path and frequency independent, the shape of the acceleration spectrum, $A(f)$, at high frequencies can be modelled by the equation:

$$A(f) = A_0 \exp\left(\frac{\pi t f}{Q}\right)$$

where f is frequency greater than the frequency, f_e, above which the dominant trend is one of exponential decay, A_0 depends on the source properties, geometrical spreading, etc., and t is travel time. This formulation assumes that the source displacement spectrum is proportional to f^{-2} (e.g. Brune, 1970; Madariaga, 1976). A plot of log $A(f)$ against f would show a straight line decay after f_e from which the gradient of the fitted straight line can be used to calculate Q.

Some of the acceleration spectra did not exhibit this linear decay at high frequencies but for six events which did, an average Q of 189 ± 67 was obtained. Source parameters for all the earthquakes were recalculated from spectra that had been corrected for whole-path attenuation with the Q value of 189 and using the transfer function $\exp(-\pi f t / Q)$. On average, the low-frequency spectral levels and the corner frequencies increased by 31 and 26%, respectively, while the high-frequency spectral level decreased by about 62%. Thus, although attenuation does have some effect on the spectra of these earthquakes, given the uncertainties inherent in the assumed models used to determine source parameters, the changes observed after correction for Q are not considered very significant.

5. Discussion

While most of the other volcanic islands of the Lesser Antilles arc have been the sites of recent earthquake sequences, this June 1992 earthquake sequence seems to have been the first, relatively significant one close to Saba for a very long time. Based on the magnitude differential of 0.7 between the two largest earthquakes, the Saba sequence may be classified as a swarm instead of a foreshock–mainshock–aftershock sequence. An important and relevant question is whether this swarm was of volcanic or tectonic origin.

Although the release of elastic strain energy in areas of recent volcanism, igneous intrusion and geothermal activity commonly occurs in the form of earthquake swarms (Eiby, 1966; Sykes, 1970), it is often impossible, in most situations, to tell whether or not the swarm is associated with movement of magma at depth. Furthermore, swarms also occur in non-volcanic environments (e.g., Frankel et al., 1980). Consequently, this cannot be used to draw any conclusions as to whether the Saba swarm was of volcanic or tectonic origin.

The Saba events have been located close to but not directly beneath the island and seem to exhibit a SW–NE trend. This spatial variation may not be totally attributable to location errors because S − P times at SAB averaged about 1.94 s. The waveforms of the Saba events are similar to those of typical tectonic or volcano-tectonic earthquakes and there was no evidence of harmonic tremor. Thus the spatial and temporal pattern of the swarm, with focal depth extending up to 25 km for the largest event, seem to preclude a volcanic origin. The swarm may be the result of a reactivation of faults in the area by regional stress.

The *b*-value of 0.74 calculated for the Saba swarm is low compared to the high values (> 1.5) reported for some confirmed volcanic swarms (e.g., Einarsson and Brandsdottir, 1980; McNutt and Bevan, 1984). A *b*-value of about 1 is typical for most seismic zones (Richter, 1958, p. 359). Mogi (1963) has attributed large *b*-values to a higher degree of heterogeneity of the subsurface material while Scholz (1968) concludes that the *b*-value is more of an indicator of the state of stress in the source region, with high *b*-values being associated with low stress conditions and vice versa. Some studies have suggested that *b*-values in volcanic areas are higher than those in tectonic environments (e.g., Ward and Matumoto, 1967; Minakami, 1974). Utsu (1971) has also concluded that *b*-values are usually higher for swarms than for earthquakes in general. However, it must be pointed out that the low *b*-value for the Saba swarm does not necessarily preclude magma as a triggering mechanism although the released strains may have been of tectonic origin.

The source parameters of the Saba swarm earthquakes cannot also be used as conclusive distinguishing characteristics as to its origin. For example, both small magnitude tectonic and volcano-tectonic earthquakes are expected to generate spectra with high corner frequencies. The earthquakes of the Saba swarm all have relatively high corner frequencies.

During the period of occurrence of these earthquakes, no indication was found on the island that an abnormal amount of heat was reaching the surface. Temperatures and rates of discharge of hot springs were stable, no fumaroles were found and temperatures in the abandoned Sulphur Mine appeared normal.

6. Conclusions

In June 1992, a minor earthquake swarm occurred close to Saba, the northernmost member of the active segment of the Lesser Antilles arc. Several of these events were felt on Saba, with the largest event which occurred on 11 June 1992, and was of magnitude M_D 4.5, being felt at MMI IV–V on Saba and III on St. Kitts. A detailed study of the characteristics of the sequence does not furnish conclusive proof but seems to suggest that the sequence was probably of tectonic rather than volcanic origin. Furthermore, it must be emphasized that the swarm should not necessarily be interpreted as representing a precursory phenomenon to more important developments in volcanic activity on Saba.

Acknowledgements

We wish to thank the staff members of the Seismic Research Unit for their help in data processing and in producing this paper: in particular, Mrs. Yvonne Joseph was responsible for typing and Mr. Godfrey Almorales for drafting some of the diagrams. Appreciation must also be extended to the people of Saba for their hospitality during our stay on their beautiful island. We are grateful to Profs. Raoul Madariaga and Pall Einarsson for their constructive reviews.

References

Aki, K., 1967. Scaling law of seismic spectrum. J. Geophys. Res., 72: 1217–1231.

Aki, K., 1984. Evidence of magma intrusion during the Mammoth Lake earthquakes of May 1980 and implication of the absence of volcanic (harmonic) tremor. J. Geophys. Res., 89: 7689–7696.

Aki, K. and Richards, P.G., 1980. Quantitative Seismology: Theory and Methods. Freeman, San Francisco, CA.

Ambeh, W.B. and Fairhead, J.D., 1991. Spectral characteristics and source parameters of microearthquakes from the Mt. Cameroon volcanic region, West Africa. Geophys. J. Int., 106: 229–237.

Anderson, J.G. and Hough, S.E., 1984. A model for the shape of the Fourier amplitude spectrum of acceleration at high frequencies. Bull. Seismol. Soc. Am., 74: 1969–1993.

Archuleta, R., Cranswick, E., Mueller, C. and Spudich, P., 1982. Source parameters of the 1980 Mammoth Lakes, California, earthquake sequence. J. Geophys. Res., 87: 4595–4607.

Bakun, W.H., Bufe, C.G. and Stewart, R.M., 1976. Body wave spectra of central California earthquakes. Bull. Seismol. Soc. Am., 66: 439–459.

Barquero, R., Alvarado, G.E. and Matumoto, T., 1992. Arenal Volcano (Costa Rica) premonitory seismicity. In: P. Gasparini, R. Scarpa, and K. Aki (Editors), Volcanic Seismology. IAVCEI Proceedings in Volcanology, 3. Springer-Verlag, Berlin, pp. 84–96.

Beckles, D.M. and Shepherd, J.B., 1988. Programs for earthquake location, data archiving and related functions using microcomputers. Spec. Publ. Seismic Research Unit, U.W.I., St. Augustine, Trinidad 1988/1, 257 pp.

Beckles, D.M., Shepherd, J.B. and Aspinall, W.P., 1977. The WURSTMACHINE: A program for estimating hypocentral coordinates of regional earthquakes. Proc. I Congr. Latino Americano de Geofisica, 1977, Caracas, 12 pp.

Boatwright, J., 1980. A spectral theory for circular seismic sources: simple estimates of source dimension, dynamic stress drop and radiated energy. Bull. Seismol. Soc. Am., 70: 1–26.

Brune, J.N., 1970. Tectonic stress and the spectra of seismic shear waves from earthquakes. J. Geophys. Res., 75: 4997–5009.

Del Pezzo, E., De Natale, G., Martini, M. and Zollo, A., 1987. Source parameters of microearthquakes at Phlegraean fields (Southern Italy) volcanic area. Phys. Earth Planet. Inter., 47: 25–42.

Eiby, G.A., 1966. Earthquake swarms and volcanism in New Zealand. Bull. Volcanol., 29: 61–74.

Einarsson, P. and Brandsdottir, B., 1980. Seismic evidence for lateral magma intrusion during the July 1978 deflation of the Krafla volcano in NE Iceland. J. Geophys., 47: 160–165.

Evison, F.F., 1977. Precursory seismic sequences in New Zealand. N. Z. J. Geol. Geophys., 20: 129–141.

Filson, J., Simkin, T. and Leu, L., 1973. Seismicity of a Caldera collapse: Galapagos Islands 1968. J. Geophys. Res., 78: 8591–8622.

Fletcher, J.B., 1980. Spectra from high dynamic range digital recordings of Oroville, California, aftershocks and their source parameters. Bull. Seismol. Soc. Am., 70: 735–755.

Frankel, A., 1982. The effects of attenuation and site response on the spectra of microearthquakes in the northeastern Caribbean. Bull. Seismol. Soc. Am., 72: 1379–1402.

Frankel, A., McCann, W.R. and Murphy, A.J., 1980. Observations from a seismic network in the Virgin Islands region: tectonic structures and earthquake swarms. J. Geophys. Res., 85: 2669–2678.

Gutenberg, B. and Richter, C.F., 1954. Seismicity of the Earth and Associated Phenomena. Princeton Univ. Press, Princeton, NJ.

Iio, Y., 1992. Seismic source spectrum of microearthquakes. Bull. Seismol. Soc. Am., 82: 2391–2409.

LADLE Study Group, 1983. A lithospheric refraction profile in the western North Atlantic ocean. Geophys. J. R. Astron. Soc., 75: 23–69.

Latter, J.H., 1979. Volcanological observations at Tongariro National Park, 2. Types and classification of volcanic earthquakes, 1976–1978. NZDSIR, Geophys. Div. Rep. 150.

Madariaga, R., 1976. Dynamics of an expanding circular fault. Bull. Seismol. Soc. Am., 66: 639–666.

McNutt, S.R. and Bevan, R.J., 1984. Patterns of earthquakes and the effect of the solid earth and ocean tides at Mount St. Helens prior to the May 18, 1980 eruption. J. Geophys. Res., 89: 3075–3086.

Minakami, T., 1974. Seismology of volcanoes in Japan. In: L. Civetta, P. Gasparini, G. Luongo and A. Rapolla (Editors), Physical Volcanology. Elsevier, Amsterdam, pp. 1–27.

Mogi, K., 1963. Some discussions on aftershocks, foreshocks and earthquake swarms—the fracture of a semi-infinite body caused by an inner stress origin and its relation to the earthquake phenomena, 3. Bull. Earthquake Res. Inst. Tokyo Univ., 41: 615–658.

Mori, J., McKee, C., Talai, B. and Itikarai, I., 1989. A summary of precursors to volcanic eruptions in Papua New Guinea. In: J.H. Latter (Editor), Volcanic Hazards: Assessment and Monitoring. (IAVCEI Proceedings in Volcanology, 1.) Springer-Verlag, Berlin, pp. 260–291.

Murphy, A.J. and McCann, W.R., 1979. Preliminary results from a new seismic network in the northeastern Caribbean. Bull. Seismol. Soc. Am., 69: 1479–1513.

Pearson, C., 1982. Parameters and a magnitude moment relationship from small earthquakes observed during hydraulic fracturing experiments in crystalline rocks. Geophys. Res. Lett., 9: 404–407.

Richter, C.F., 1958. Elementary Seismology. Freeman, San Francisco, CA.

Roobol, M.J. and Smith, A.L., 1989. Volcanic and associated hazards in the Lesser Antilles. In: J.H. Latter (Editor), Volcanic Hazards: Assessment and Monitoring. (IAVCEI Proceedings in volcanology, 1.) Springer-Verlag, Berlin, pp. 57–85.

Roobol, M.J., Smith, A.L. and Tomblin, J.F., 1994. An assessment of the volcanic hazard on the islands of Saba and St. Eustatius in the northern Lesser Antilles. Confidential Rep. Rijks Geol. Dienst, 205 pp.

Sawada, Y., Tanaka, Y. and Seino, M., 1989. Volcanic activity in Japan monitored by the Japan Meteorological Agency using detected precursory phenomena. In: J.H. Latter (Editor), Volcanic Hazards: Assessment and Monitoring. (IAVCEI Proceedings in Volcanology, 1.) Springer-Verlag, Berlin, pp. 246–259.

Scherbaum, F. and Kisslinger, C., 1984. Variations of apparent stresses and stress drops prior to the earthquake of 6 May 1984 ($m_b = 5.8$) in the Adak seismic zone. Bull. Seismol. Soc. Am., 74: 2577–2592.

Scholz, C.H., 1968. The frequency–magnitude relation of micro-fracturing in rock and its relation to earthquakes. Bull. Seismol. Soc. Am., 58: 399–415.

Shepherd, J.B. and Aspinall, W.P., 1983. Seismicity and earthquake hazard in Trinidad and Tobago, West Indies. Earthquake Eng. Struct. Dyn., 11: 229–250.

Smith, A.L. and Roobol, M.J., 1994. Eastern Caribbean Volcanic Hazards. In: W.B. Ambeh (Editor), Proceedings of the Caribbean Conference on Natural Hazards: Volcanoes, Earthquakes, Windstorms and Floods (in press).

Sykes, L.R., 1970. Earthquake swarms and sea floor spreading. J. Geophys. Res., 75: 6598–6611.

Thatcher, W. and Hanks, T.C., 1973. Source parameters of southern California earthquakes. J. Geophys. Res., 78: 8547–8576.

Tucker, B. and Brune, J., 1977. Source mechanism and m_b–M_s analysis of aftershocks of the San Fernando earthquake. Geophys. J. R. Astron. Soc., 49: 371–426.

Utsu, T., 1971. Aftershocks and earthquake statistics III. J. Fac. Sci., Hokkaido Univ., Ser. VII, 3: 379–441.

Ward, P.L. and Matumoto, T., 1967. A summary of volcanic and seismic activity at Katmai National Monument, Alaska. Bull. Volcanol., 31: 107–129.

Westermann, J.H. and Kiel, H., 1961. The geology of Saba and St. Eustatius. Uitg. Natuurwet. Stud. Suriname Ned. Antillen 24, 175 pp.

Zobin, V.M., 1979. Variations of earthquake source parameters before volcanic eruptions. J. Volcanol. Geotherm. Res., 9: 311–334.

Zobin, V.M. and Gorelchik, V.I., 1982. Seismicity and source parameters of earthquakes in the region of the large Tolbachik fissure eruption. Bull. Volcanol., 45: 99–113.